SCIENTIFIC REPORTS

OPEN

Tunable Open Circuit Voltage by Engineering Inorganic Cesium Lead Bromide/Iodide Perovskite Solar Cells

Received: 10 October 2017
Accepted: 10 January 2018
Published online: 06 February 2018

Chi Huey Ng[1,2], Teresa S. Ripolles[2], Kengo Hamada[2], Siow Hwa Teo[1,2], Hong Ngee Lim[1,3], Juan Bisquert[4,5] & Shuzi Hayase[2]

Perovskite solar cells based on series of inorganic cesium lead bromide and iodide mixture, $CsPbBr_{3-x}I_x$, where *x* varies between 0, 0.1, 0.2, and 0.3 molar ratio were synthesized by two step-sequential deposition at ambient condition to design the variations of wide band gap light absorbers. A device with high overall photoconversion efficiency of 3.98 % was obtained when small amount of iodide ($CsPbBr_{2.9}I_{0.1}$) was used as the perovskite and *spiro*-OMeTAD as the hole transport material (HTM). We investigated the origin of variation in open circuit voltage, V_{oc} which was shown to be mainly dependent on two factors, which are the band gap of the perovskite and the work function of the HTM. An increment in V_{oc} was observed for the device with larger perovskite band gap, while keeping the electron and hole extraction contacts the same. Besides, the usage of bilayer P3HT/MoO_3 with deeper HOMO level as HTM instead of *spiro*-OMeTAD, thus increased the V_{oc} from 1.16 V to 1.3 V for $CsPbBr_3$ solar cell, although the photocurrent is lowered due to charge extraction issues. The stability studies confirmed that the addition of small amount of iodide into the $CsPbBr_3$ is necessarily to stabilize the cell performance over time.

Perovskite solar cells have attracted great attention as the prime energy conversion devices, owing to its reasonably low fabrication cost without compromising its photovoltaic performances. Relentless efforts have been done to optimize the parameters of perovskite solar cell for high power conversion efficiency (PCE) purpose, typically the hybrid organic-inorganic methylammonium lead halide ($CH_3NH_3PbX_3$ or $MAPbX_3$, where X is a halide Cl, Br, I, or mixture of halides) which has accomplished PCE over 20%[1–3]. Particularly, the mixture of halides in perovskite solar cells were envisioned to be able to adjust the absorption spectra which may be an advantageous property for full spectrum energy harvesting and photoelectrochemical applications. By tuning the iodide/bromide ratio of the mixed halides perovskite solar cell such as the increment of iodide concentration led to red-shifting of the absorption range and thereby, enhances the photovoltaic performance. Under this scenario, Seok and co-workers reported a PCE of 12.3 % for the $MAPb(I_{1-x}Br_x)_3$ perovskite solar cell and manifested the feasibility in obtaining excellent photovoltaic performances by manipulating the ratio between halides of I^- and Br^-[4]. Similar performances were also obtained from Huang and co-workers for an inverted $MAPb(I_{1-x}Br_x)_3$ architecture, using a bilayer of indene-C_{60} tri-adducts (ITCA) and C_{60} as electron transport materials[5]. Even, hybrid iodide/bromide perovskite hole conductor free solar cells showed good stability and efficiencies of 8.54 %[6]. In addition, a $MAPb(I_{1-x}Br_x)_3$ solar cell prepared through vacuum deposition technique by Bolink and co-workers achieved an efficiency of 10.2 %[7]. However, aforementioned perovskite possesses restriction on stability and therefore, researchers replace the conventional organic cation (MA^+) to inorganic cation such as cesium (Cs^+). Thermogravimetric analyses confirm that the inorganic perovskite, cesium lead bromide ($CsPbBr_3$) has higher

[1]Department of Chemistry, Faculty of Science, Universiti Putra Malaysia, 43400 UPM, Serdang, Selangor, Malaysia. [2]Graduate School of Life Science and Systems Engineering, Kyushu Institute of Technology, 2-4 Hibikino, Wakamatsu-ku, Kitakyushu, 808-0196, Japan. [3]Functional Device Laboratory, Institute of Advanced Technology, Universiti Putra Malaysia, 43400 UPM, Serdang, Selangor, Malaysia. [4]Institute of Advanced Materials (INAM), Universitat Jaume I, 12006, Castelló, Spain. [5]Department of Chemistry, Faculty of Science, King Abdulaziz University, Jeddah, Saudi Arabia. Correspondence and requests for materials should be addressed to T.S.R. (email: teresa@life.kyutech.ac.jp) or J.B. (email: bisquert@uji.es) or S.H. (email: hayase@life.kyutech.ac.jp)

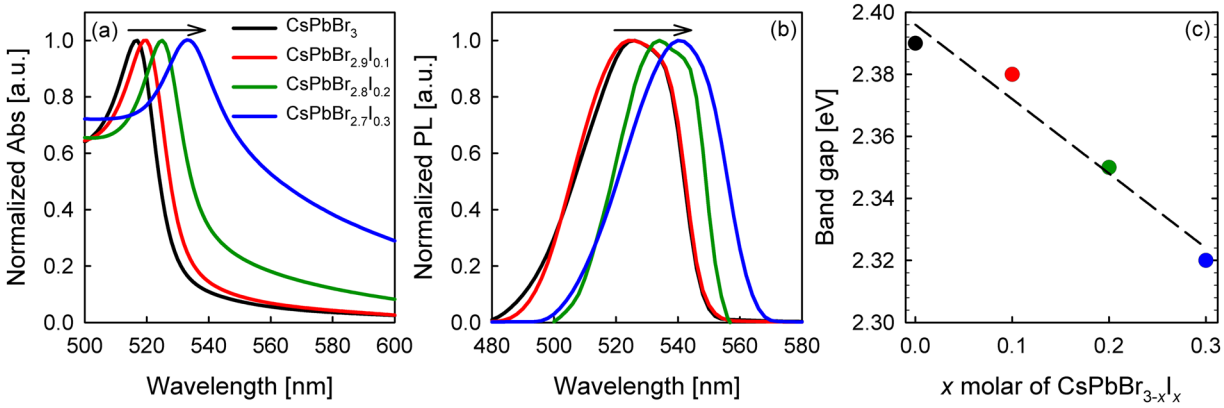

Figure 1. Normalized (**a**) absorption (Abs) and (**b**) photoluminescence (PL) of $CsPbBr_{3-x}I_x$, where x is 0, 0.1, 0.2, and 0.3 in molar ratio. The intersection between Abs and PL spectra represents the (**c**) band gap energy.

thermal stability than the hybrid organic-inorganic perovskite, $MAPbBr_3$[8]. Additionally, $CsPbBr_3$ exhibits good charge transport properties with an electron mobility of ~1000 cm^2/Vs and electron lifetime of 2.5 μs[9,10]. Whereas, $CsPbI_3$ perovskite solar cells show enhancement in optical and electrical properties[11]. So far, the photoconversion efficiencies of both perovskite solar cells are poor due to low charge carrier collection of $CsPbBr_3$[8], and structural changes of $CsPbI_3$ perovskite at room temperature. Despite $CsPbI_3$ perovskite solar cell fabricated under vacuum-processed has achieved high efficiency of 10.5 %, subsequently the improved efficiency of mixed halides or mixed halide-mixed Pb/Sn perovskite solar cells up to 11 % has been reported, however, the need of high technology equipment such as vacuum chamber and glove box during the fabrication process have restrained its outdoor applications competency owing to unsolved stability issue and high production cost[12–15]. Therefore, a mixture of halides cesium perovskite absorber material, $CsPbBr_{3-x}I_x$ is a suitable harvester candidate to improve the optical and electrical properties, subsequently enhances the cell performance and stability performance.

Generally, high open circuit voltage V_{oc} is one of the photovoltaic parameters to be achieved for high overall photoconversion efficiencies. The factors that control the V_{oc} are the adequate match of the Lowest Unoccupied Molecular Orbital (LUMO) level of the electron transport material (ETM) and the conduction band of the perovskite layer, as well as the Highest Occupied Molecular Orbital (HOMO) level of the hole transport material (HTM) and the valence band of the perovskite layer[16]. However, other studies predicted that the V_{oc} is closely related to the charge recombination rate and the work functions of the HTMs[17–19]. An example that confirms this theory where the V_{oc} of $TiO_2/MAPbI_3$ layer covered with copper iodide (CuI) as the *p*-type semiconductor was reduced, as opposed to other devices without this layer. This behavior was attributed to higher recombination processes[20]. Other reports also confirm that the V_{oc} is solely determined by the perovskite absorber, regardless of the TiO_2 surface modifications such as TiO_2-coating with a thin film of MgO in order to change the conduction band[21]. Furthermore, an inverted perovskite solar cell using conducting polymers as the hole-selective contact materials exhibited direct correlation between higher work functions of HTM and lower charge recombination rate, consequently the V_{oc} was increased[17,19]. Interesting results were recently obtained for $MAPbBr_3$-based solar cells with mesoporous-TiO_2 scaffold layer. Two HTMs, a novel molecule based on 1,3,4- oxadiazole ring (H1) and the standard *spiro*-OMeTAD with different HOMO levels of −5.43 and −5.22 eV, respectively were compared. The device prepared with H1 achieved a V_{oc} of 1.43 V and was further increased to 1.49 V with the usage of *spiro*-OMeTAD for solar cell devices. The authors confirm that there was not a clear correlation between HOMO level of the $MAPbBr_3$ (−5.9 eV) and work function of the HTMs[22]. Therefore, in-depth study to further improve the V_{oc} and efficiency performance is still continuing. However, it is notable that the V_{oc} is originated from two factors, which are the band gap of the perovskite material and the perfect matching of electron and hole transporting interface.

In this manuscript, we combine two important properties in achieving high V_{oc} in standard solar cells, which are the tunable band gap in inorganic perovskite absorbers and the capability to extract hole charge carrier properly. A number of $CsPbBr_{3-x}I_x$ perovskite absorber films were synthesized through two-step deposition technique by varying small amount of x ratio from 0 to 0.3. These films were characterized by X-ray diffraction (XRD), UV-Vis spectroscopy, photoluminescence, and ultraviolet photoelectron spectroscopy (UPS). Upon the addition of iodide into the perovskite $CsPbBr_3$ matrix, the band gap descended and consequently, the V_{oc} decreased. In addition, the HTMs pose direct effect on the V_{oc} behavior. The pure $CsPbBr_3$ solar cells reported high V_{oc} close to 1.16 V with *spiro*-OMeTAD, but increased to 1.30 V with a bilayer of $P3HT/MoO_3$. Finally, the stability issues were also analyzed in this work, concluding that small amount of iodide indeed stabilize all photovoltaic parameters.

Results and Discussion

Absorption, emission, and band gap. $CsPbBr_{3-x}I_x$ perovskites (x varies from 0 to 0.3) were synthesized through two-step sequential deposition process by spin coating different molar ratio of PbI_2:$PbBr_2$ solution, subsequently dipped in CsBr solution for perovskite formation in ambient condition. Figure 1 shows the UV-visible absorption and emission spectra of the $CsPbBr_{3-x}I_x$ perovskite films with different bromide/iodide molar ratio. Both the absorption and emission spectra display red-shifted trend towards longer wavelength as the iodide

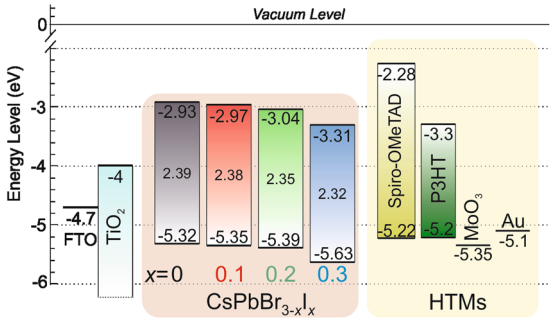

Figure 2. Schematic energy level diagram of a complete TiO_2-mesoporous $CsPbBr_{3-x}I_x$ (x is 0, 0.1, 0.2 or 0.3) perovskite solar cell, employing either *spiro*-OMeTAD[34] or P3HT/MoO_3[32,35] as the hole transporting material. The band gap of each perovskite, where x is 0, 0.1, 0.2, and 0.3 was also indicated.

concentration of the $CsPbBr_{3-x}I_x$ perovskite films increases, as illustrated in Figure 1a and 1b. The lower absorption coverage of a purely bromide film could be ascribed to the bromide ion, which narrows the vibration mode and band near-IR region[23]. The band gap (E_g) of each perovskite material was calculated via equation (1),

$$E_g = \frac{1240}{\lambda} \quad (1)$$

where E_g refers to the band gap and λ is the intersected wavelength of the UV-Vis and photoluminescence. To be specific, the wavelength obtained from the intersection point between UV-Vis and photoluminescence was inserted into equation (1) in determining the band gap of each perovskite material, as summarized in Figure 1c. When the amount of PbI_2 in $CsPbBr_3$ matrix increases, gradual reduction in E_g was observed from 2.39 ($CsPbBr_3$), 2.38 ($CsPbBr_{2.9}I_{0.1}$), 2.35 ($CsPbBr_{2.8}I_{0.2}$), to 2.32 eV ($CsPbBr_{2.7}I_{0.3}$), which is in great agreement with the previous reports in the literature[4,24]. In order to complete the energy level diagram, the valence band of each $CsPbBr_{3-x}I_x$ perovskite material, $x = 0$, 0.1, 0.2, and 0.3, respectively, was measured through ultraviolet photoelectron spectroscopy (UPS), as shown in Figure S1. The HOMO levels have recorded the values of −5.52, −5.35, −5.60, and −5.61 eV, corresponding to $CsPbBr_{3-x}I_x$, where $x = 0$, 0.1, 0.2, and 0.3, respectively, as manifested in Figure 2.

Crystallinity and morphological structure. The crystallinity of the perovskite films was investigated via XRD to study the crystal phase transition of the perovskite materials. The temperature dependent $CsPbX_3$ perovskite material could be existed in three polymorphic structures, either in tetragonal, orthorhombic, or in cubic structure. Interestingly, at high annealing temperature of 350 °C, the transformation of $CsPbX_3$ material into cubic phase was observed from the XRD profile (Figure S2). The experimental peaks are closely matches the theoretical $CsPbBr_3$ peaks (JCPDS file #00–054–0752) and are in agreement with other reported works in the literature[8,25,26]. The highly crystalline peaks at 15.2°, 21.6°, and 30.6° are indexed to (100), (110), and (200), respectively. In addition, some additional low intensity peaks detected from 22° to 30° are corresponded to the non-reacted $PbBr_2$. The intensity of the $PbBr_2$ peaks was diminished and even disappeared owing to the $PbBr_2$ has been completely substituted by PbI_2 when the concentration of iodide increases. The presence of low intensity peak of CsBr was also detected at 30° in all perovskite films due to synthesis of perovskite film was through two-step sequential deposition. The XRD profile explicates an unnoticeable blue-shifted trend to lower angles region as the concentration of iodide increases. This is owing to the substitution of larger iodide ions over the bromide lattice, which expanded the d-spacing of the halide matrix and thus inversely brought to lower degree detection[14]. Figure S3 shows the FE-SEM images of $CsPbBr_{3-x}I_x$ perovskite films. Pinholes (yellow arrow) are observed on the surface of $CsPbBr_3$ perovskite film where the formation of voids could be due to evaporation of organic solvent during annealing process. Whereas, upon the inclusion of iodide anion, the compactness of the perovskite is gradually improved with the presentation of pinhole-free surface, as shown in Figure S3(b–d). Figure S3d shows the alteration of perovskite structure of $CsPbBr_{2.7}I_{0.3}$ (observation of non-homogenized morphological surface) when 0.3 molar ratio of iodide was incorporated within bromide matrix, which could be due to the overloading of iodide anion.

Photovoltaic performances. The photovoltaic performances of different bromide/iodide ratios solar cell, employing $CsPbBr_{3-x}I_x$ (x varies from 0, 0.1, 0.2, and 0.3 molar ratio) as the perovskite layer and *spiro*-OMeTAD as the HTM were measured under 1 sun (AM1.5G 100 $mWcm^{-2}$) illumination and dark conditions, as depicted in Figure 3 and the corresponding photovoltaic results were tabulated in Table 1.

Taking into account of all photovoltaic parameters, the addition of minute amount of iodide has dramatically improved the photoconversion efficiency of $CsPbBr_3$ from 2.97 % to 3.98 % for $CsPbBr_{2.9}I_{0.1}$ solar cell with high open circuit voltage (V_{oc}) of 1.13 V and fill factor (FF) of 0.64. Similar photovoltaic results were also observed for $CsPbBr_{2.8}I_{0.2}$ device. Nevertheless, further increasing the iodide amount in $CsPbBr_{3-x}I_x$ did not improve the cell performance. Contrary, the photoconversion efficiency plunged to 2.73 % when 0.3 molar ratio of iodide was incorporated to the bromide matrix. The performance differences were dependent on the short circuit current (J_{sc}) and FF; while keeping the V_{oc} almost constant (Figure 3a). The substantial reduction of FF for $CsPbBr_{2.7}I_{0.3}$

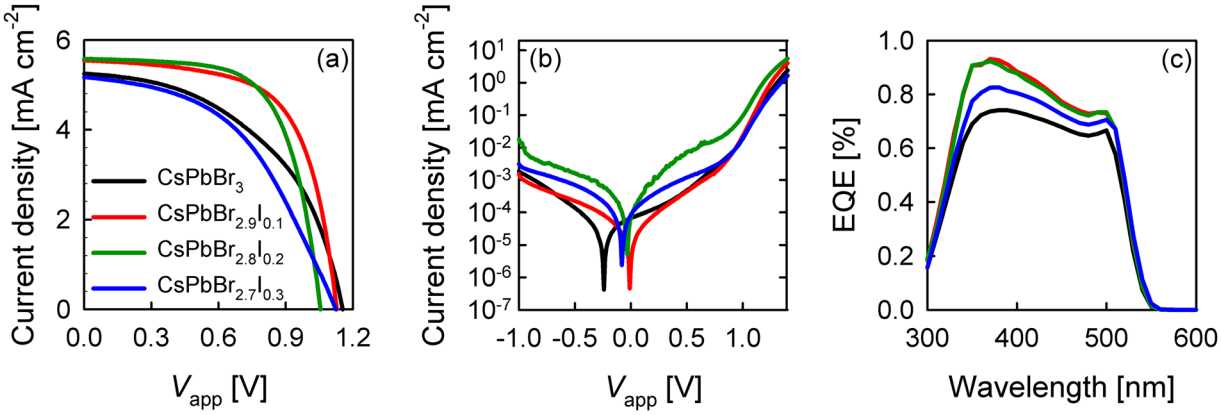

Figure 3. (**a**) J-V measurements under simulated AM1.5G sun light of 100 mW cm^{-2} irradiance, and (**b**) under dark. (**c**) Represents the EQE for glass/FTO/c-TiO_2/mp-TiO_2/$CsPbBr_{3-x}I_x$/*spiro*-OMeTAD/Au solar cells, where *x* varies in 0, 0.1, 0.2, and 0.3 molar ratio.

Perovskite	V_{oc} (V)	J_{sc} (mA/cm^2)	*FF*	PCE (%)	J_{sc}[Cal.] (mA/cm^2)	R_{sh}, kΩ/cm^2	R_s, Ω/cm^2	HI
$CsPbBr_3$	1.16	5.25	0.49	2.97	5.85	220.3	2711	0.11
$CsPbBr_{2.9}I_{0.1}$	1.13	5.54	0.64	3.98	6.83	294.5	1674	0.04
$CsPbBr_{2.8}I_{0.2}$	1.06	5.58	0.65	3.83	6.78	673.0	1724	0.0002
$CsPbBr_{2.7}I_{0.3}$	1.12	5.17	0.47	2.73	6.44	158.5	5194	0.08

Table 1. Photovoltaic parameters of the $CsPbBr_{3-x}I_x$ solar cells (*x* varies between 0, 0.1, 0.2, and 0.3 in molar ratio) with *spiro*-OMeTAD as the HTM. The photocurrent calculated from the integration of the EQE curves was also added. Hysteresis index (HI) was calculated by equation (2).

solar cell could be attributed to the occurrence of minor interfacial charge recombination, which resulted from relatively higher series and lower shunt resistances, as manifested in Table 1. The J-V curves under dark at −1 V reflected small differences between devices (Figure 3b) implies suppressed charge recombination[27]. The J_{sc} and *FF* parameters were improved when the iodide concentration was either in 0.1 or 0.2 molar ratio ($CsPbBr_{2.9}I_{0.1}$ or $CsPbBr_{2.8}I_{0.2}$) relative to $CsPbBr_3$ and $CsPbBr_{2.7}I_{0.3}$ perovskite solar cells. These results imply that higher amount of iodide disturbs the charge extraction of the cell and thus only an optimized amount of PbI_2 is favorable. Figure 3c shows the external quantum efficiency (EQE) spectra of $CsPbBr_{3-x}I_x$ devices and the results are consistent with the J_{sc} performance. The EQE intensity increases from 350 nm to 500 nm upon the addition of iodide into the pure $CsPbBr_3$. The current calculated from the integration of the EQE curves demonstrated the occurrence of some recombination mechanisms that affect these devices, consequently reduced the J_{sc} performance. Figure S4 shows the enlarged EQE spectrum of $CsPbBr_{3-x}I_x$ based perovskite devices. It can be seen that there are noticeable shifts of EQE onset to longer wavelengths in conjunction with the iodide increment, which is in great agreement with the absorption spectra in Figure 1.

Hysteresis effects are first to be investigated for cesium-based perovskite solar cell with mixed halide architecture, as manifested in Figure S5. The hysteresis index (HI) was obtained via equation (2)[11,28].

$$\frac{J_{RS}(0.5V_{oc}) - J_{FS}(0.5V_{oc})}{J_{RS}(0.5V_{oc})} \quad (2)$$

where $J_{RS}(0.5V_{oc})$ and $J_{FS}(0.5V_{oc})$ represent the photocurrent density at 50% of V_{oc} for the reverse (RS) and forward (FS) scan directions, respectively. As a reference HI is 0 when no hysteresis was observed, while HI of 1 represents the case where the hysteresis is as high as the magnitude of the photocurrent. It shows that the hysteretic performance of the $CsPbBr_{3-x}I_x$, where $x = 0.1–0.3$ perovskite devices is alleviated with the inclusion of iodide, as compared to the purely $CsPbBr_3$ device with a HI value of 0.11. Considering the hysteretic performance of the champion cell ($CsPbBr_{2.9}I_{0.1}$) against $CsPbBr_3$, hysteresis index was doubly reduced to 0.04 when 0.1 molar ratio of iodide was incorporated. It hence implies that mitigation of hysteretic effect can be done not only through cation engineered, but also through halides architecture, which should be the next research focus.

There are two factors that are able to tune the V_{oc} performance of a perovskite solar cell, which are the band gap of the halide mixture perovskite material and the employment of different work function HTM, as manifested in Figure 4. Analyzing solar cells of different perovskite band gap, the V_{oc} should be improved for the solar cells with larger perovskite band gap rather than narrower band gap. Figure 4a and 4b illustrated the V_{oc} behavior of a perovskite solar cell towards a narrower and a wider perovskite band gap, respectively. It shows that small V_{oc} increment was observed when a device with larger perovskite band gap was used; taking the hole and electron transport materials the same. Due to the addition of minute amount of iodide within the $CsPbBr_{3-x}I_x$ matrix, and a consequence of small shift on band gap (ΔE_g), the V_{oc} changed slightly under these circumstances.

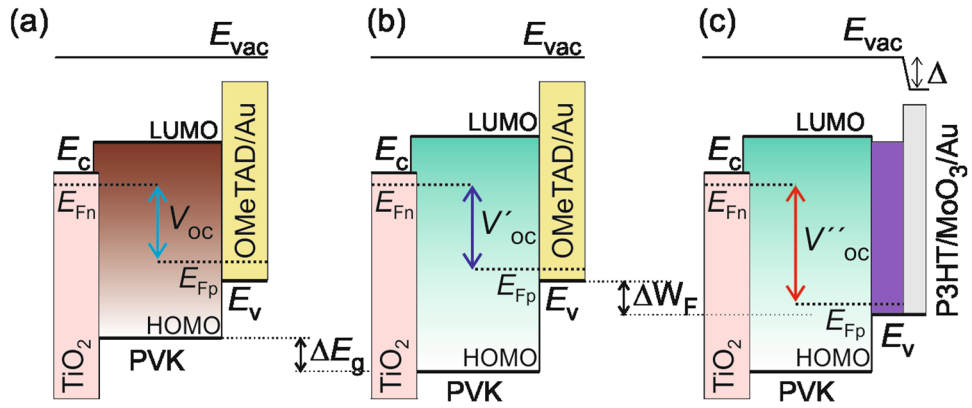

Figure 4. The V_{oc} behavior of the perovskite solar cells is represented in the energy level diagrams by employing (**a**) narrow or (**b**) wide band gaps (E_g) perovskite absorber, and (**c**) different HTMs, such as *spiro*-OMeTAD/Au in (**a**) and (**b**) or deeper work function (W_F) P3HT/MoO_3/Au in (**c**). The conduction band (E_c), valence band (E_v), Fermi level of electrons (E_{Fn}) and holes (E_{Fp}) were indicated. The MoO_3 layer creates a dipole (Δ) at the interface, reducing the vacuum level energy (E_{vac}). The Au performs as the electron blocking layer.

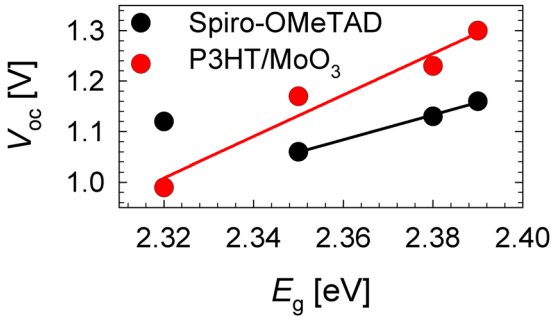

Figure 5. Band gap dependence of open circuit voltage in devices with different $CsPbBr_{3-x}I_x$ perovskite compositions and HTM such as *spiro*-OMeTAD or P3HT/MoO_3.

Despite the photovoltaic devices employing *spiro*-OMeTAD as the HTM performed high V_{oc} close to 1.1 V, nevertheless, it was expected to achieve even higher V_{oc} values with the usage of wide band gap perovskite materials. To gain further insight on V_{oc} tuning and subsequently, the performance of the photovoltaic device, the choice of hole extractor is an another factor to be considered besides the perovskite absorbers. When a bilayer polymer/oxide (P3HT/MoO_3) was used as the HTM, the V_{oc} was drastically improved from 1.16 V to 1.3 V, as manifested in Figure S6 and Table S1 owing to deeper HOMO energy level of P3HT/MoO_3 than *spiro*-OMeTAD. The offsets of HOMO level between P3HT-perovskite in the range of 0.1–0.4 eV merited the hole extraction process. Moreover, the inclusion of MoO_3 interlayer between P3HT and Au performs as exciton blocking layer, herein retards reverse charge flow[29]. Figure 4c shows that the P3HT-based solar cells with the same perovskite materials shifted the hole Fermi level (E_{Fp}) to lower energy level, hence enhanced the V_{oc} considerably. In all cases, the V_{oc} enhancement was observed for the P3HT/MoO_3 devices, as compared to the *spiro*-OMeTAD devices, except for $CsPbBr_{2.7}I_{0.3}$ solar cell. This situation is similar to the large V_{oc} increment obtained in dye-sensitized solar cells when using redox couple with more positive redox potential[30]. Figure S6c illustrates the EQE spectra of $CsPbBr_{3-x}I_x$ devices using P3HT/MoO_3 as the HTM were correlating well with the J_{sc} performances. All in all, it thus confirmed that the origin of the V_{oc} is depending on both the band gap of the perovskites and the work function of the HTMs. Photovoltaic performances of champion $CsPbBr_{3-x}I_x$ solar cells and its average photovoltaic performances of five solar devices, coupled with the error bars are depicted in Figure S7 and Table S2.

Figure 5 shows the linear dependency between V_{oc} and band gap (E_g) of $CsPbBr_{3-x}I_x$ perovskite absorbers using different HTMs, *spiro*-OMeTAD and P3HT/MoO_3. This pattern is more pronouncing for the case of P3HT because P3HT has a deeper HOMO level than *spiro*-OMeTAD. Nevertheless, the $CsPbBr_{2.7}I_{0.3}$-based solar cell with E_g of 2.32 eV did not follow the mentioned tendency, which may be due to the HOMO level collected from the UPS is much deeper in energy level (−5.61 eV) than the other $CsPbBr_{3-x}I_x$ perovskites and thus was excluded from the linear fitting of Figure 5.

There is another point of view to explain the photovoltaic response of these materials. A solar cell is composed of sequence of materials, carefully chosen with different work functions in order to extract the photoinduced charge carrier efficiently. Thus, larger differences in the work function of P3HT/MoO_3, as compared to the *spiro*-OMeTAD using the same perovskite layer for both cases were studied. The first case (*spiro*-OMeTAD)

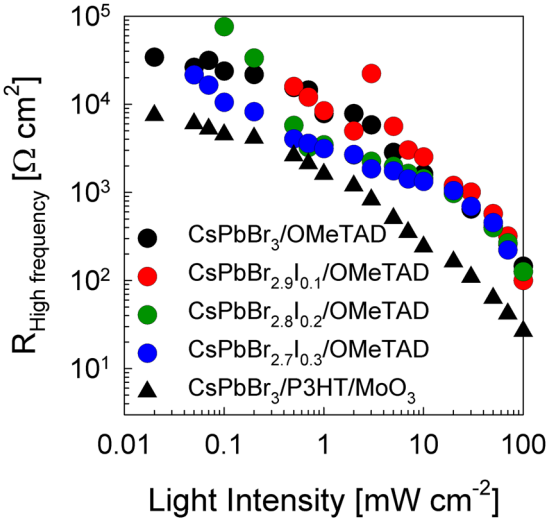

Figure 6. Resistance fitted at high frequency range in impedance spectroscopy measured at numerous light intensities from low light intensity to 1 sun illumination. Different $CsPbBr_{3-x}I_x$ perovskite compositions (x varies between 0, 0.1, 0.2, and 0.3 in molar ratio) and hole transport materials as *spiro*-OMeTAD/Au (circle dots) and P3HT/MoO_3/Au (triangle dots) were analyzed.

enabled efficient charge extraction and contributed to higher V_{oc}. However, the P3HT/MoO_3 devices showed reduction in J_{sc} in all solar cells (Figure S6a and Table S1) could be due to shorter electron lifetime of P3HT based solar cells than *spiro*-OMeTAD based solar cells. To further understand this phenomenon, additional charge loss processes at the interface of perovskite/HTM were found in the impedance spectroscopy results. Figure 6 displays the fitted resistance at different illumination intensities from 0.02 to 100 mWcm^{-2} radiation. This measurement was carried out at high frequency range in order to avoid polarization and memory effects. The equivalent circuit model to fit the impedance plot, one arc, was a simple resistance in parallel with a capacitance. Close to 1 sun illumination intensity, all $CsPbBr_{3-x}I_x$/*spiro*-OMeTAD solar cells showed the same resistance pattern, independent of the composition of the perovskite layer. Small amount of iodide unaltered the above resistance. However, when the HTM was changed to P3HT/MoO_3 for $CsPbBr_3$-based solar cell, the resistance dropped considerably at the same charge carrier or light intensity. This effect was correlated to the reduction of the J_{sc} observed in the J-V curves. This behavior means that the resistance at the interface between perovskite/HTM detected variations when the contact changed, namely *spiro*-OMeTAD and P3HT/MoO_3, but was constant when the perovskite composition ($CsPbBr_{3-x}I_x$) changed. As a matter of fact, it was observed in Figure 2 that the effective LUMO of P3HT/MoO_3 was rather close to perovskite absorber E_v energy, indicating that the driving force for hole carrier extraction was small. This feature lead to charge accumulation at the interface, which increases the recombination and thereby, the loss of photocurrent occurred (Figure S6a).

Another important factor to be studied is the stability performance of the devices when a small amount of PbI_2 was added to synthesize $CsPbBr_{3-x}I_x$ perovskite solar cells. The measurements were carried out in ambient air with a thin film of polymethylmethacrylate, PMMA, deposited on the Au surface for encapsulation purpose. Thus, oxygen and water factors were to be omitted. The performance was measured for six days and between measurements, the devices were kept in the glove box under nitrogen ambient and dark conditions. Aging analysis of $CsPbBr_{3-x}I_x$ solar cells are summarized in Figure 7.

The $CsPbBr_3$- and $CsPbBr_{2.7}I_{0.3}$-based devices showed steady decay in *FF* and more pronounced in J_{sc} with constant V_{oc}. The decrease of J_{sc} for $CsPbBr_{2.9}I_{0.1}$ and $CsPbBr_{2.8}I_{0.2}$ solar cells was less drastic, whilst the *FF* and V_{oc} remain constant. There are several reasons to explain the reduction of J_{sc}, as observed in all devices. The *spiro*-OMeTAD solution used as a HTM was composed of 4-*tert*-butylpyiridine as an additive, which may react with the perovskite layer[31]. Another additive used in the previous solution was *bis* (trifluoromethane) sulfonimide lithium salt (Li-TFSI) which increases the hole mobility and conductivity, but the cell stability can be affected by the oxidation process[32]. Or even, some studies confirm that the mesoporous-TiO_2 created additional deep traps due to oxygen desorption at the surface caused by the UV-illumination[33]. It is important to highlight that small addition of iodide into the $CsPbBr_3$ not merely improved the photoconversion efficiencies from 0.66 % for $CsPbBr_3$ to 3.53 % for $CsPbBr_{2.9}I_{0.1}$ after 6 days but also its stabilities. Contrary, high amount of PbI_2 such as $CsPbBr_{2.7}I_{0.3}$ perovskite damaged the absorber composition over time, resulted an efficiency of 1.16 % after 6 days. Other important factor to consider is the selective HTM in perovskite solar cells. The P3HT/MoO_3/Au layer acted as a stabilizer in the solar cells, keeping all photovoltaic parameters constant over time. The large V_{oc} (>1.3 V) achieved for the $CsPbBr_3$/P3HT/MoO_3-based solar cell highlights that this material is promising for its numerous applications.

Conclusions

In summary, we reported a complete film and device characterization for $CsPbBr_{3-x}I_x$ perovskite where x varies between 0, 0.1, 0.2, and 0.3 molar ratio, and the absorbers fall in large band gap's category, specifically more than

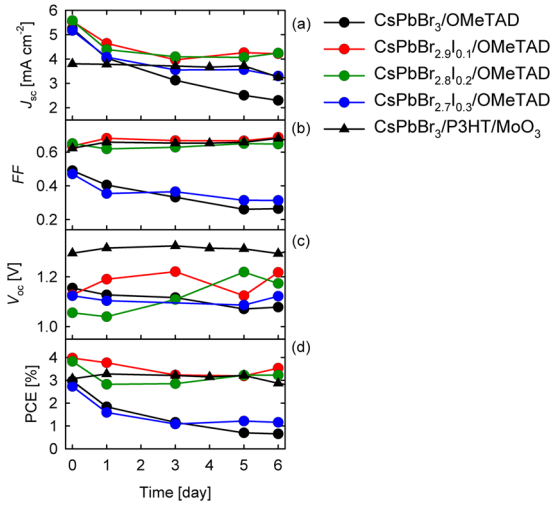

Figure 7. Aging analysis of $CsPbBr_{3-x}I_x$ devices (x varies between 0, 0.1, 0.2, and 0.3 molar ratio). Figures show the cell parameters (**a**) J_{sc}, (**b**) *FF*, (**c**) V_{oc}, and (**d**) efficiency as a function of time.

2.3 eV. All-inorganic perovskite solar cell based on small amount of iodide $CsPbBr_{2.9}I_{0.1}$ as the absorber and *spiro*-OMeTAD as the HTM prepared in ambient condition achieved well-performance of 3.98 % efficiency, as opposed to 2.97 % for pure $CsPbBr_3$ perovskite. Likewise, the addition of optimized amount of iodide (0.1 molar ratio) has successfully mitigated the hysteretic performance of $CsPbBr_{2.9}I_{0.1}$ perovskite solar cell, as compared to $CsPbBr_3$ device. We concluded that there are two main factors to explain the origin of the V_{oc} in lead halide perovskite solar cells, which are the large band gap of the absorber and the deep hole selective transport material which are important for V_{oc} increment. Regarding the perovskite layer, improvement in the V_{oc} was observed when the band gap of the $CsPbBr_{3-x}I_x$ perovskite increases, independent of the HTM used. In particular, the increment of V_{oc} was more pronouncing for P3HT/MoO_3-based solar cell, as opposed to the *spiro*-OMeTAD based solar cell due to lower work function property of P3HT/MoO_3. Additionally, the V_{oc} was also affected by the selected HTM. When the *spiro*-OMeTAD was substituted by P3HT/MoO_3, an increment of V_{oc} from 1.16 V to 1.3 V was obtained. However, J_{sc} was reduced due to the charge extraction issues, which is observable from the impedance spectroscopy measurements. Stability operation shows that the $CsPbBr_{2.9}I_{0.1}$ and $CsPbBr_{2.8}I_{0.2}$-based solar cells possessed better stability than the pure bromide and $CsPbBr_{2.9}I_{0.1}$ solar cells when *spiro*-OMeTAD was used as the HTM. Whilst, the perovskite solar cells showed no significant decay for the P3HT/MoO_3 contact.

Experimental section

Materials. The fluorine-doped tin oxide (FTO) glass substrate with a size of 2.5×2.5 cm^2 was purchased from Nippon Sheet Glass Co. Ltd (10 Ω/sq). The mesoporous titanium dioxide (mp-TiO_2) was obtained from JGC Catalysts and Chemicals Ltd (PST-18NR) and was diluted with α-terpineol (Wako) (1:3 by weight). The perovskite films were prepared through two sequential deposition process. The pure $CsPbBr_3$ perovskite film was prepared from a thin film of lead (II) bromide ($PbBr_2$, > 98%) from Sigma-Aldrich. Additionally, small amount of lead (II) iodide (PbI_2, > 98%) purchased from TCI Tokyo Chemical Industry CO., LTD, was added into the $PbBr_2$ solution in order to synthesize a mixture of $PbBr_2$:PbI_2 in the molar ratio of 1:0, 1:0.1, 1:0.2, and 1:0.3. These solutions were dissolved with dimethlyformamide DMF (Sigma-Aldrich). Then, these films were dipped into a solution of cesium bromide (CsBr, 99.9%) obtained from Alfa Aesar, which dissolved in methanol (Wako) in a concentration of 15 mg/mL. For the hole transport materials (HTMs), 2,2′,7,7′-tetrakis[N,N-di(4-methoxyphenyl)amino]-9,9′-spirobifluorene, *spiro*-OMeTAD, obtained from Sigma-Aldrich was dissolved in chlorobenzene (purchased from Sigma-Aldrich). In order to improve its electrical properties, some additives were added, such as *bis* (trifluoromethane) sulfonimide lithium salt (Li-TFSI) dissolved with acetonitrile (520 mg/mL, Wako) and 4-*tert*-butylpyridine (TBP) which purchased from Sigma-Aldrich and TCI, respectively. Poly(3-hexylthiophene-2,5-diyl), P3HT, acquired from Sigma-Aldrich was dissolved in *o*-dichlorobenzene (Sigma-Aldrich) with a concentration of 17 mg/mL.

Device fabrication. The FTO-coated glass was patterned using HCl (6 M)-etched with Zn powder and cleaned by firstly, ultrasonification in a basic bath of neutral water, acetone, isopropanol, and deionized water and secondly, plasma system for several minutes. A 20 nm of compact titanium dioxide (c-TiO_2) prepared from titanium diisopropoxide bis (acetylacetonate) was deposited through atomic layer deposition method at 300 °C. The mesoporous layer mp-TiO_2 was spin coated onto c-TiO_2 surface at the spinning conditions of 500 rpm for 3 s and 6000 rpm for 30 s, followed by an immediate heating at 80 °C for 10 min, subsequently was calcined at 470 °C for 30 min. The synthesis of perovskite film was conducted via two-steps sequential method. Firstly, an aliquot of 90 μL $PbBr_2$:PbI_2, being a molar ratio of 1:0, 1:0.1, 1:0.2, and 1:0.3, was initially spin coated onto mp-TiO_2 surface at 2500 rpm for 1 min. These films were heated at 75 °C for 30 min on a hot plate. Secondly, the $PbBr_2$:PbI_2 coated films were dipped into CsBr solution for 10 min at 50 °C, subsequently washed with 2-propanol solution for 1 min at 50 °C. The $CsPbBr_{3-x}I_x$ films were synthesized after annealing at 350 °C for 10 min. Subsequently,

spiro-OMeTAD was spin coated on the surface of perovskite film at 500 rpm for 3 s, later 4000 rpm for 30 s. The films were left to dry inside a petri dish about 15 h in dark. No annealing treatments were required. On the other hand, the P3HT samples were prepared through spin coating process at 1000 rpm for 10 min. Drying procedure were finished after 16 h storage inside a petri dish in dark and then, an annealing treatment at 130 °C for 10 min was carried out. Finally, an 8 nm MoO_3 film was thermally evaporated for P3HT-based solar cells, and 60 nm of Au was deposited for all devices.

Materials characterization. The glass/FTO/$CsPbBr_{3-x}I_x$ substrates (where x varies between 0, 0.1, 0.2, and 0.3 in molar ratio) were characterized by several techniques. The UV-Visible spectra was performed via JASCO V-670 spectrophotometer from 200–900 nm. The emission spectra were obtained from JASCO FP- 6600 spectrofluorometer from 450–600 nm. The valence band of perovskite was measured through Ultraviolet Photo Electron Spectroscopy (UPS) (BUNKOUKEIKI). The X-Ray diffraction (XRD) was conducted through RINT-Ultima III, Rigaku in 2θ range from 14 to 50 degrees using monochromatic CuK_α radiation. The surface morphologies of the perovskite materials were investigated using a Quanta 400F FE-SEM equipped with an EDX feature.

Device characterization. The current density-voltage (J-V) plot was measured by a solar simulator (CEP-2000SRR, Bunkoukeiki Inc) with light source intensity of AM1.5G 100 $mWcm^{-2}$, which was calibrated with a reference silicon cell. All solar cells were measured using a mask with active area of 0.12 cm^2 under 1 sun. The photovoltaic measurements were carried out at a scan rate of 0.1 Vs^{-1} with 100 ms delay time and 10 mV voltage step. The measurement of external quantum efficiency (EQE) was performed through CEP-2000SRR, Bunko Keiki with 300 W Xe lamp. The monochromator was adjusted to 1×10^{16} $mWcm^{-2}$ and was monitored by Si photodiode. The impedance spectroscopy at open circuit conditions was measured with a potentiostat (AUTOLAB PGSTAT204 connected to an impedance module FRA32M) in a range of frequencies from 1 MHz to 10 Hz in a perturbation amplitude of 0.01 V. Different light intensities were analyzed from 0.02 to 100 $mWcm^{-2}$.

References

1. Hutter, E. M., Eperon, G. E., Stranks, S. D. & Savenije, T. J. Charge carriers in planar and meso-structured organic–inorganic perovskites: mobilities, lifetimes, and concentrations of trap states. *J. Phys. Chem. Lett.* **6**, 3082–3090, https://doi.org/10.1021/acs.jpclett.5b01361 (2015).
2. Lee, M. M., Teuscher, J., Miyasaka, T., Murakami, T. N. & Snaith, H. J. Efficient hybrid solar cells based on meso-superstructured organometal halide perovskites. *Science* **338**, 643–647 (2012).
3. Green, M. A., Emery, K., Hishikawa, Y., Warta, W. & Dunlop, E. D. Solar cell efficiency tables (version 47). *Prog. Photovolt: Res. Appl.* **24**, 3–11, https://doi.org/10.1002/pip.2728 (2016).
4. Noh, J. H., Im, S. H., Heo, J. H., Mandal, T. N. & Seok, S. I. Chemical management for colorful, efficient, and stable inorganic–organic hybrid nanostructured solar cells. *Nano Lett.* **13**, 1764–1769 (2013).
5. Bi, C., Yuan, Y., Fang, Y. & Huang, J. Low-Temperature Fabrication of Efficient Wide-Bandgap Organolead Trihalide Perovskite Solar Cells. *Adv. Energy Mater.* **5** (2015).
6. Aharon, S., Cohen, B. E. & Etgar, L. Hybrid lead halide iodide and lead halide bromide in efficient hole conductor free perovskite solar cell. *J. Phys. Chem. C* **118**, 17160–17165 (2014).
7. Gil-Escrig, L., Miquel-Sempere, A., Sessolo, M. & Bolink, H. J. Mixed Iodide–Bromide Methylammonium Lead Perovskite-based Diodes for Light Emission and Photovoltaics. *J. Phys. Chem. Lett.* **6**, 3743–3748, https://doi.org/10.1021/acs.jpclett.5b01716 (2015).
8. Kulbak, M. *et al.* Cesium Enhances Long-Term Stability of Lead Bromide Perovskite-Based Solar Cells. *J. Phys. Chem. Lett.* **7**, 167–172, https://doi.org/10.1021/acs.jpclett.5b02597 (2016).
9. Stoumpos, C. C. *et al.* Crystal Growth of the Perovskite Semiconductor $CsPbBr_3$: A New Material for High-Energy Radiation Detection. *Cryst. Growth Des.* **13**, 2722–2727, https://doi.org/10.1021/cg400645t (2013).
10. Kulbak, M., Cahen, D. & Hodes, G. How Important Is the Organic Part of Lead Halide Perovskite Photovoltaic Cells? Efficient $CsPbBr_3$ Cells. *J. Phys. Chem. Lett.* **6**, 2452–2456, https://doi.org/10.1021/acs.jpclett.5b00968 (2015).
11. Ripolles, T. S., Nishinaka, K., Ogomi, Y., Miyata, Y. & Hayase, S. Efficiency enhancement by changing perovskite crystal phase and adding a charge extraction interlayer in organic amine free-perovskite solar cells based on cesium. *Sol. Energy Mater. Sol. Cells* **144**, 532–536, https://doi.org/10.1016/j.solmat.2015.09.041 (2016).
12. Frolova, L. A. *et al.* Highly Efficient All-Inorganic Planar Heterojunction Perovskite Solar Cells Produced by Thermal Coevaporation of CsI and PbI_2. *J. Phys. Chem. Lett.* **8**, 67–72, https://doi.org/10.1021/acs.jpclett.6b02594 (2017).
13. Niezgoda, J. S., Foley, B. J., Chen, A. Z. & Choi, J. J. Improved Charge Collection in Highly Efficient $CsPbBrI_2$ Solar Cells with Light-Induced Dealloying. *ACS Energy Lett.* **2**, 1043–1049, https://doi.org/10.1021/acsenergylett.7b00258 (2017).
14. Beal, R. E. *et al.* Cesium Lead Halide Perovskites with Improved Stability for Tandem Solar Cells. *J. Phys. Chem. Lett.* **7**, 746–751, https://doi.org/10.1021/acs.jpclett.6b00002 (2016).
15. Liang, J. *et al.* $CsPb_{0.9}Sn_{0.1}IBr_2$ Based All-Inorganic Perovskite Solar Cells with Exceptional Efficiency and Stability. *J. Am. Chem. Soc.* **139**, 14009–14012, https://doi.org/10.1021/jacs.7b07949 (2017).
16. Ryu, S. *et al.* Voltage output of efficient perovskite solar cells with high open-circuit voltage and fill factor. *Energy Environ. Sci.* **7**, 2614–2618, https://doi.org/10.1039/C4EE00762J (2014).
17. Yan, W. *et al.* Increasing open circuit voltage by adjusting work function of hole-transporting materials in perovskite solar cells. *Nano Res.* **9**, 1600–1608 (2016).
18. Suarez, B. *et al.* Recombination Study of Combined Halides (Cl, Br, I) Perovskite Solar Cells. *J. Phys. Chem. Lett.* **5**, 1628–1635, https://doi.org/10.1021/jz5006797 (2014).
19. Yan, W. *et al.* High-performance hybrid perovskite solar cells with open circuit voltage dependence on hole-transporting materials. *Nano Energy* **16**, 428–437, https://doi.org/10.1016/j.nanoen.2015.07.024 (2015).
20. Christians, J. A., Fung, R. C. & Kamat, P. V. An inorganic hole conductor for organo-lead halide perovskite solar cells. Improved hole conductivity with copper iodide. *J. Am. Chem. Soc.* **136**, 758–764 (2013).
21. Gouda, L. *et al.* Open circuit potential build-up in perovskite solar cells from dark conditions to 1 sun. *J. Phys. Chem. Lett.* **6**, 4640–4645 (2015).
22. Carli, S. *et al.* A New 1, 3, 4-Oxadiazole-Based Hole-Transport Material for Efficient $CH_3NH_3PbBr_3$ Perovskite Solar Cells. *ChemSusChem* **9**, 657–661 (2016).
23. Dimesso, L., Dimamay, M., Hamburger, M. & Jaegermann, W. Properties of $CH_3NH_3PbX_3$ (X = I, Br, Cl) Powders as Precursors for Organic/Inorganic Solar Cells. *Chem. Mater.* **26**, 6762–6770, https://doi.org/10.1021/cm503240k (2014).

24. Wang, B., Xiao, X. & Chen, T. Perovskite photovoltaics: a high-efficiency newcomer to the solar cell family. *Nanoscale* **6**, 12287–12297, https://doi.org/10.1039/C4NR04144E (2014).
25. Chen, X. *et al*. $CsPbBr_3$ perovskite nanocrystals as highly selective and sensitive spectrochemical probes for gaseous HCl detection. *J. Mater. Chem. C* **5**, 309–313, https://doi.org/10.1039/C6TC04136A (2017).
26. Protesescu, L. *et al*. Nanocrystals of Cesium Lead Halide Perovskites ($CsPbX_3$, X = Cl, Br, and I): Novel Optoelectronic Materials Showing Bright Emission with Wide Color Gamut. *Nano Lett.* **15**, 3692–3696, https://doi.org/10.1021/nl5048779 (2015).
27. Zhu, Q. *et al*. Compact Layer Free Perovskite Solar Cells with a High-Mobility Hole-Transporting Layer. *ACS Appl. Mater. Interfaces* **8**, 2652–2657 (2016).
28. Chen, H.-W., Sakai, N., Ikegami, M. & Miyasaka, T. Emergence of Hysteresis and Transient Ferroelectric Response in Organo-Lead Halide Perovskite Solar Cells. *J. Phys. Chem. Lett.* **6**, 164–169, https://doi.org/10.1021/jz502429u (2015).
29. Wang, Z. *et al*. Copolymers based on thiazolothiazole-dithienosilole as hole-transporting materials for high efficient perovskite solar cells. *Org. Electron.* **33**, 142–149, https://doi.org/10.1016/j.orgel.2016.03.020 (2016).
30. Feldt, S. M. *et al*. Design of organic dyes and cobalt polypyridine redox mediators for high-efficiency dye-sensitized solar cells. *J. Am. Chem. Soc.* **132**, 16714–16724 (2010).
31. Zhao, X. & Park, N.-G. In *Photonics*. 1139–1151 (Multidisciplinary Digital Publishing Institute).
32. Pho, T. V. *et al*. Decacyclene Triimides: Paving the Road to Universal Non-Fullerene Acceptors for Organic Photovoltaics. *Adv. Energy Mater.* **4**, 1301007–n/a, https://doi.org/10.1002/aenm.201301007 (2014).
33. Leijtens, T. *et al*. Overcoming ultraviolet light instability of sensitized TiO_2 with meso-superstructured organometal tri-halide perovskite solar cells. *Nat. Comm.* **4** (2013).
34. Jeon, N. J. *et al*. o-Methoxy Substituents in Spiro-OMeTAD for Efficient Inorganic–Organic Hybrid Perovskite Solar Cells. *J. Am. Chem. Soc.* **136**, 7837–7840, https://doi.org/10.1021/ja502824c (2014).
35. Irfan *et al*. Energy level evolution of air and oxygen exposed molybdenum trioxide films. *Appl. Phys. Lett.* **96**, 116 (2010).

Acknowledgements

This work has been supported by KAKENHI from the Japan Society for the Promotion of Science (JSPS) under the Grant-in-Aid for Young Scientists B (Grant Number JP16K17947) and by MINECO of Spain under project MAT2016–76892-C3-1-R.

Author Contributions

S.H. and T.S.R., contributed to the conception and design of the experiment. C.H.N., T.S.R. and K.H. carried out film preparation and characterization, device fabrication and performance measurements. S.H.T. concluded the X.R.D. measurements and analysis of the data. C.H.N. and T.S.R. analyzed data and wrote the manuscript with the assistance of H.N.L., J.B., and S.H. Impedance spectroscopy was measured by T.S.R. and analyzed the data with assistance of J.B.

Additional Information

Supplementary information accompanies this paper at https://doi.org/10.1038/s41598-018-20228-0.

Competing Interests: The authors declare that they have no competing interests.

Publisher's note: Springer Nature remains neutral with regard to jurisdictional claims in published maps and institutional affiliations.